Spectral phonon mean free path and thermal conductivity accumulation in defected graphene: The effects of defect type and concentration

Tianli Feng,[1] Xiulin Ruan,[1,*] Zhenqiang Ye,[2] and Bingyang Cao[2,†]

[1]*School of Mechanical Engineering and the Birck Nanotechnology Center, Purdue University, West Lafayette, Indiana 47907-2088, USA*

[2]*Key Laboratory for Thermal Science and Power Engineering of Ministry of Education, Department of Engineering Mechanics, Tsinghua University, Beijing 100084, People's Republic of China*

(Received 18 February 2015; published 4 June 2015)

The spectral phonon properties in defected graphene have been unclear due to the lack of advanced techniques for predicting the phonon-defect scattering rate without fitting parameters. Taking advantage of the extended phonon normal mode analysis, we obtained the spectral phonon relaxation time and mean free path (MFP) in defected graphene and studied the impacts of three common types of defects: Stone-Thrower-Wales (STW) defect, double vacancy (DV), and monovacancy (MV). The phonon-STW defect scattering rate is found to have no significant frequency dependence, and as a result, the relative contribution of long-wavelength phonons sharply decreases. In contrast, the phonon scattering by DVs or MVs exhibits a frequency dependence of $\tau_{p-d}^{-1} \sim \omega^{1.1-1.3}$ except for a few long-wavelength phonons, revisiting the traditionally used $\sim\omega^4$ dependence. We note that although MV-defected graphene has the lowest thermal conductivity as compared to the other two defected graphene samples at the same defect concentration, it has a portion of phonons with the longest MFP. The contribution from the long-MFP and long-wavelength phonons does not decrease much as the vacancy concentration increases. STW defect and MV block more out-of-plane modes than in-plane modes, while DV has less bias for which mode to block. As the MV concentration increases from 0 to 1.1%, the relative contribution from out-of-plane modes decreases from 30% to 18%, while that of the transverse acoustic mode remains at around 30%. These findings of spectral phonon properties can provide more insight than the effective properties and benefit the prospective phononic engineering.

DOI: 10.1103/PhysRevB.91.224301 PACS number(s): 63.22.Rc, 63.20.kg, 63.20.kp, 65.80.Ck

I. INTRODUCTION

Defects in the two-dimensional material graphene have attracted extensive attention in recent years for their properties and functionalities [1]. The simplest and most common point defects in graphene are Stone-Thrower-Wales (STW) defects [2], double vacancies (DV), and monovacancy (MV), which have been directly observed in experiments [3–9]. Due to the imperfection of practical techniques, these defects are produced inevitably during the process of growth and processing of samples [3]. Quantitative study of the impact of these defects on thermal transport in graphene is of great importance, because it can provide effective guidance on intentionally manufactured graphene for desired functionalities in the application of thermal management and thermoelectrics [10–14].

The thermal conductivity κ of point defected single layer graphene (SLG) has been extensively investigated using molecular dynamics (MD) and nonequilibrium Green's function (NEGF). The results vary with the employed interatomic potentials and calculation methods. Zhang *et al.* [15] found that thermal conductivity in graphene was reduced by almost 98% by introducing 1% MVs using equilibrium MD (EMD) with Green-Kubo method (GK-MD). With a different interatomic potential, Hao *et al.* [16] predicted a reduction of about 85% with the same method. They also compared the MV defect with the STW defect and found that the latter gave a 77% reduction in κ at the same concentration. Similarly, Mortazavi and Ahzi [17] predicted a 74% reduction in κ by 1% STW defects using the nonequilibrium MD (NEMD) method. They compared the impact of those defects on κ and found that, with the same defect concentration, the thermal conductivity in STW-defected graphene is slightly higher than DV-defected graphene, which is then marginally higher than MV-defected graphene. With the NEMD method, Haskins *et al.* [18] compared the impact of STW defects, DVs, and MVs on κ of the graphene nanoribbon (GNR) and found that κ was reduced by 70% in 0.1% STW or DV defected GNR and 80% in 0.1% MV defected GNR. In contrast, Yeo *et al.* [19] found the reduction of κ in GNR was about 80% at a defect concentration of 10%. Jiang *et al.* [20] also noticed that the vacancy position significantly affected the thermal transport in GNR using the NEGF method. Other impacts of defects on thermal properties in GNR such as quantum thermal transport [21] and thermal rectification [22] have also been studied.

Although extensive work has been done on predicting the thermal conductivity in defected materials, the spectral phonon relaxation time and MFP are still not available. This is due to the lack of advanced techniques for predicting spectral phonon scattering rate by defects such as vacancies and dislocations, although significant advances have been achieved in predicting phonon-phonon, phonon-isotope, and phonon-boundary scattering [23]. The bond distortion, adding or missing around the defects, makes phonon-defect scattering currently hard to calculate. Typically the phonon-defect scattering rate is fitted as $\sim\omega^4$ [23], however the accuracy of this dependence is still an open issue because it was derived from the long-wavelength approximation [24–27]. Very recently Xie *et al.* [28] calculated the phonon scattering rate by the missing bonds around vacancies in graphene

*ruan@purdue.edu

†caoby@tsinghua.edu.cn

using Klemens' formalism [24,25], which depends on fitting parameters and long-wavelength approximation, and thus the accuracy is unwarrantable. Since prospective phononic engineering technique requires a modulation of thermal transport by phonon with different ranges of wavelength and frequency, it is necessary to have a deep understanding of the spectral phonon MFP in defected materials [23]. Therefore, to develop a reliable approach for predicting the phonon scattering rate by various types of defects is of great importance.

In this paper, we study the impact of various types of defects with different concentrations on the phonon relaxation time, MFP, and mode-wise thermal conductivity. We extend the normal mode analysis (NMA) [23,29–32] from predicting phonon-phonon scattering rate in pristine systems to calculating the total phonon scattering rate in defected materials. The defected graphene is assumed to have the same phonon dispersion with pristine graphene. The anharmonicity and the defects are treated together as a perturbation to phonon normal modes, and as a result, the linewidth of spectral energy density (SED) gives the total scattering rate covering phonon-phonon and phonon-defect scattering rates. This paper is organized as follows. The methodologies for calculating the phonon MFP and mode-wise thermal conductivity are introduced in Sec. II. In Sec. III, we compare the impact of various types of defects with the same concentration in graphene on the thermal conductivity (Sec. III A), spectral phonon relaxation time and MFP (Sec. III B), κ accumulation with phonon wavelength (Sec. III C), κ accumulation with phonon MFP (III D), and the relative importance of phonon branches (Sec. III E). Furthermore, we fix the defect type as MV and study the impact of the concentration on spectral phonon properties in Sec. IV. A summary and further discussion are presented in Sec. V.

II. METHODOLOGY AND SIMULATION SETUP

The atomic structures of STW defect, DV, and MV are shown in Fig. 1, in which the ^{13}C isotope is sketched as a reference. STW defect is introduced by rotating two adjacent atoms by 90°. DV and MV are produced by removing two adjacent atoms and a single atom, respectively. To study the impact of different types of defects on the phonon transport in graphene, we fixed the concentration of defects at 1.1%, which is the same concentration as natural ^{13}C. The 1.1% isotope-doped and defected SLG samples are shown in Fig. 1, in which the defects are randomly distributed and nonconnected.

To investigate the phonon relaxation time and mode-wise thermal conductivity of those defected SLG, we refer to NMA based on EMD [23,29–32]. The NMA is carried out by evaluating the normal mode coordinates [33] and the spectral energy density $\Phi_{\mathbf{k},\nu}(\omega)$:

$$q_{\mathbf{k},\nu}(t) = \sum_{\alpha}^{3}\sum_{b}^{n}\sum_{l}^{N_c}\sqrt{\frac{m_b}{N_c}}u_{\alpha}^{l,b}(t)e_{b,\alpha}^{\mathbf{k},\nu *}\exp\left[i\mathbf{k}\cdot\mathbf{r}_0^l\right], \quad (1)$$

$$\Phi_{\mathbf{k},\nu}(\omega) = |\mathcal{F}[\dot{q}_{\mathbf{k},\nu}(t)]|^2 = \frac{C_{\mathbf{k},\nu}}{\left(\omega-\omega_{\mathbf{k},\nu}^A\right)^2+\left(\tau_{\mathbf{k},\nu}^{-1}\right)^2/4}. \quad (2)$$

In Eq. (1), $u_{\alpha}^{l,b}(t)$ is the αth component of the time dependent displacement of the bth basis atom in the lth unit cell, N_c is the total number of unit cells, e^* denotes the complex conjugate of phonon eigenvector, and $\mathbf{r}_0$ is the equilibrium position. $\mathbf{k}$ and ν label the phonon mode, i.e., the phonon wave vector and phonon polarization branch, respectively. The SED function $\Phi_{\mathbf{k},\nu}(\omega)$ is obtained by performing Fourier transform $\mathcal{F}$ on the time derivative of q. As shown in Eq. (2), $\Phi_{\mathbf{k},\nu}(\omega)$ is a Lorentzian function with peak position $\omega_{\mathbf{k},\nu}^A$ and full width $\tau_{\mathbf{k},\nu}^{-1}$ at half maximum, and $C_{\mathbf{k},\nu}$ is a constant for a given mode $(\mathbf{k},\nu)$. From MD simulation the time dependent atomic velocity $\dot{u}$ is obtained and substituted into Eqs. (1) and (2), and then the spectral phonon scattering rate $\tau_{\mathbf{k},\nu}^{-1}$ is obtained by fitting the SED function to a Lorentzian function.

NMA was previously applied to calculate the phonon-phonon scattering rate in pristine materials [23], while we extend the NMA to the calculation of the total phonon scattering rate, including phonon-phonon and phonon-defect

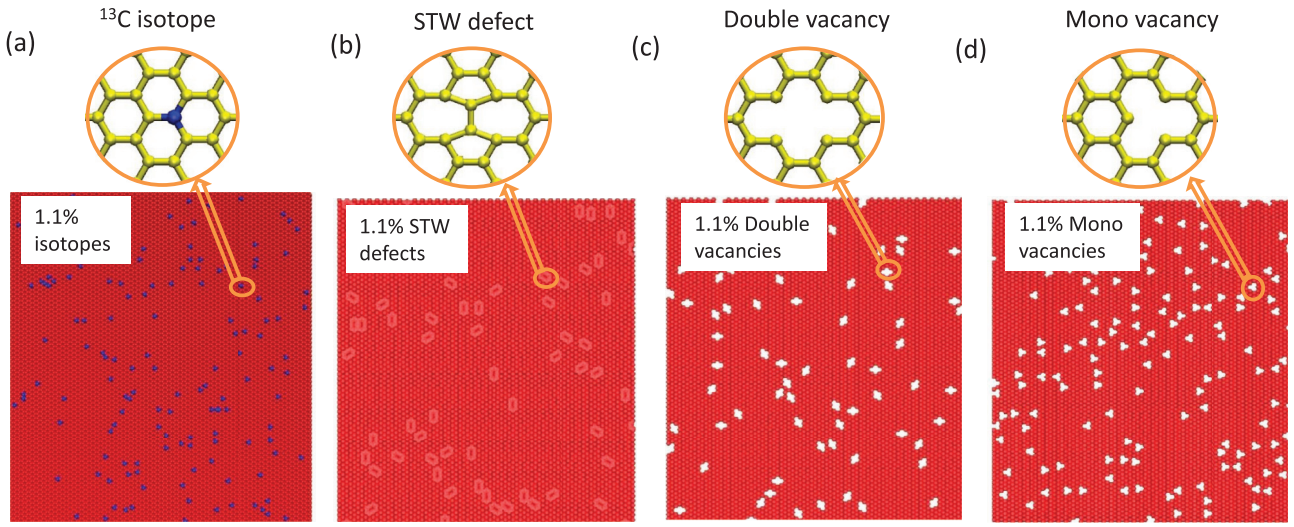

FIG. 1. (Color online) Illustrations of the structures for 1.1% (a) ^{13}C doped, (b) STW-defected, (c) double-vancancy-defected, and (d) mono-vacancy-defected SLG samples.

scattering, in defected materials. By treating anharmonicity and defects together as one perturbation to phonon normal mode, the total phonon scattering rate is read out from the linewidth of the SED function. The physical meaning of the linewidth is the amplitude of the combined perturbation from the interatomic anharmonicity and the defects. It is noted that phonon-phonon scattering and phonon-defect scattering are not necessarily independent, i.e., they may couple with each other and lead to the failure of Matthiessen's rule. Even in this case, NMA does not fail since it has nothing to do with the detailed scattering process and thus does not depend on Matthiessen's rule.

With the information of spectral phonon relaxation time, thermal conductivity κ can be calculated from the kinetic theory

$$\kappa_x = \frac{1}{V}\sum_{\mathbf{k},\nu} v^2_{\mathbf{k},\nu,x} c_{\mathbf{k},\nu}\tau_{\mathbf{k},\nu}, \tag{3}$$

where V is the volume of the sample. The summation in Eq. (3) is done over all the $3N$ resolvable phonon modes with N representing the total number of atoms in the domain. The specific heat per mode is $c = \hbar\omega\partial n^0/\partial T$, where n^0 is the phonon occupation number which is given by $n^0 = (e^\theta - 1)^{-1}$ for Bose-Einstein distribution or $n^0 = e^{-\theta}$ for classical Boltzmann distribution, and θ is the shorthand of $\hbar\omega/k_BT$. The group velocity in the x direction v_x is calculated from the dispersion relation. Since NMA only works out the relaxation time for the phonon modes in the periodic simulation directions, Eq. (3) is evaluated based on the isotropic assumption:

$$\kappa = \frac{1}{h}\frac{1}{(2\pi)}\frac{1}{2}\sum_{\nu}\int v^2_{\mathbf{k},\nu} c_{\mathbf{k},\nu}\tau_{\mathbf{k},\nu} k dk, \tag{4}$$

where h (=0.335 nm) is the thickness of SLG.

As a reference, the GK method based on EMD is performed to calculate the thermal conductivity of defected graphene:

$$\kappa_x = \frac{1}{k_BT^2V}\int_0^\infty \langle S_x(t)S_x(0)\rangle dt, \tag{5}$$

where $\langle S_x(t)S_x(0)\rangle$ is the heat current autocorrelation function (HCACF) with $S_x(t)$ representing the heat current in the x direction. The κ values in this paper are averaged in the armchair and zigzag directions.

Molecular dynamics simulations in this paper were performed using LAMMPS [34] with the optimized Tersoff potential [35] describing the interatomic interactions in graphene. The optimized Tersoff potential has been shown to produce significantly better lattice properties, such as lattice constant and phonon dispersion relation, than the original one [36] in graphene. The total simulation time and step interval are set as 10 ns and 0.5 fs, respectively. In GK-MD, the autocorrelation length is set as 100 ps which is long enough to get converged HCACF. In NMA, the atomic velocities are sampled every 5 fs which is short enough to resolve all the phonon modes. To ensure that the defects are not connecting to each other, while being adjacent is allowed, the minimum distance between any two defects is set as 6 Å. The size effect in the GK-MD method is examined by increasing the periodic simulation domain size from 5 nm × 5 nm to 40 nm × 40 nm. The GK-MD method has no significant size effect compared to NEMD [37]. It is found that κ reaches convergence after the size increases to about 10 nm × 10 nm. The results in this paper are obtained based on the size of 17 nm × 20 nm which contains 12 800 atoms. In NMA, this size sample resolves a k mesh of 80 × 80 which is dense enough to get converged thermal conductivity.

Quantum correction is required for classical MD since the room temperature is far below the Debye temperature of SLG (1000–2300 K [38]). The quantum temperature T_Q is calculated by equaling the total kinetic energy in MD to half of the total phonon energy [20]. The classical temperature in MD $T_{\mathrm{MD}} = 190$ K is found to be equivalent to the quantum temperature $T_Q = 300$ K [20], thus all the MD simulations in this paper were performed at the temperature of $T_{\mathrm{MD}} = 190$ K. In the GK method, the thermal conductivity after quantum correction is given by $\kappa_Q(T_Q) = \kappa_{\mathrm{MD}}(T_{\mathrm{MD}})dT_{\mathrm{MD}}/dT_Q$ [39]. In NMA combined with kinetic theory, $\kappa_Q(T_Q)$ is calculated by choosing the Bose-Einstein distribution at $T_Q = 300$ K to calculate the specific heat c in Eq. (4) [40].

III. COMPARISON OF VARIOUS DEFECT TYPES

A. Thermal conductivity

The thermal conductivity κ_0 of pristine SLG given by GK-MD is around 1100 W/mK after QC and 1800 W/mK before QC [40]. It is noted that this value, from EMD, is below that from NEMD based on the same interatomic potential [17,41], indicating the intrinsic difference between EMD and NEMD [37]. These k_0 values are comparable with experimental data (1500–4000 W/mK) [10,42–46] considering the uncertainty due to the sample preparation and measurement method. The accuracy of κ_0 in pristine SLG does not affect the comparative study of the impact of different defect types and concentrations in the following sections.

The relative thermal conductivities κ/κ_0 calculated from GK-MD and NMA in the defected graphene samples are shown in Fig. 2. The values from NMA are found to agree well with those from GK-MD, indicating that the assumption of treating defects as a perturbation to phonon normal mode is reasonable in graphene. The natural 1.1% ^{13}C is found to reduce κ by approximately 15%, akin to the 10–15% predicted by the ALD method [47]. This is consistent with the measured results [48] considering the uncertainty in the measured data. Compared

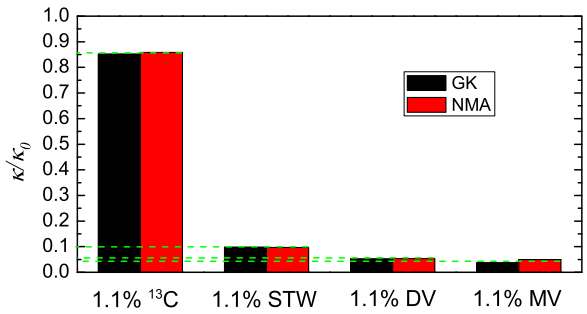

FIG. 2. (Color online) The relative thermal conductivity κ/κ_0 predicted from GK-MD and NMA-BTE in defected SLG samples at room temperature. κ_0 is the thermal conductivity of pristine SLG at room temperature.

to isotopes, the other three types of defects give much more reduction to κ. Specifically, 1.1% STW defects give the least reduction of around 90% while MVs give the most of about 95% reduction in κ. Double vacancies cause slightly less reduction in κ than single vacancies, because DV graphene has a smaller total scattering cross section considering that DV-defected graphene owns a larger scattering cross section for each scattering site but half the number of scattering sites of MV-defected graphene. These results are generally consistent with previous papers [15–17], where the detailed comparison between the κ reduction by those defects has been extensively discussed. In this paper, we are more interested in the impact of those defects on the spectral phonon relaxation time, MFP, and contribution to κ.

B. Spectral phonon relaxation time and mean free path

First of all, we investigate the phonon density of states (DOS), which is calculated by taking the Fourier transformation of the atomic velocities autocorrelation functions. DOS can qualitatively analyze the underlying influence of the defects on the thermal conductivity and is written as

$$g(\omega) = \int \exp(-i\omega t)\langle v(t)v(0)\rangle dt. \quad (6)$$

The DOS of pristine graphene and the three types of 1.1% defected graphene are illustrated in Fig. 3. On the whole, the four situations have a similar shape with a prominent peak near 48 THz, which agrees well with the characteristic of graphene [17]. Several points should be noticed. First, the value of the prominent peak in defected graphene decreases remarkably compared to that in pristine graphene. With the same defect concentration, the peak of STW-defected graphene suffers the biggest fall, and DV-defected graphene suffers the least. Second, more phonons with high frequencies (>50 THz) are excited because of the local vibration around the defects, implying the increase of the proportion of the high-frequency phonons. Third, many minor peaks at lower frequencies are damped out in defected graphene, which can reduce the relaxation times of the corresponding phonon

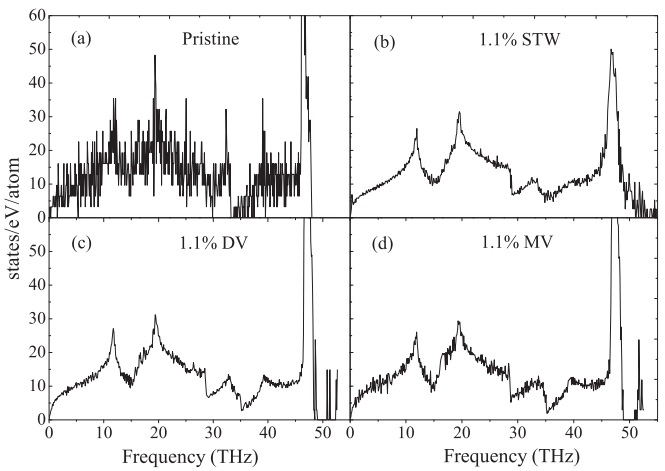

FIG. 3. The DOS of (a) pristine SLG, (b) 1.1% STW-defected SLG, (c) 1.1% DV-defected SLG, and (d) 1.1% MV-defected SLG.

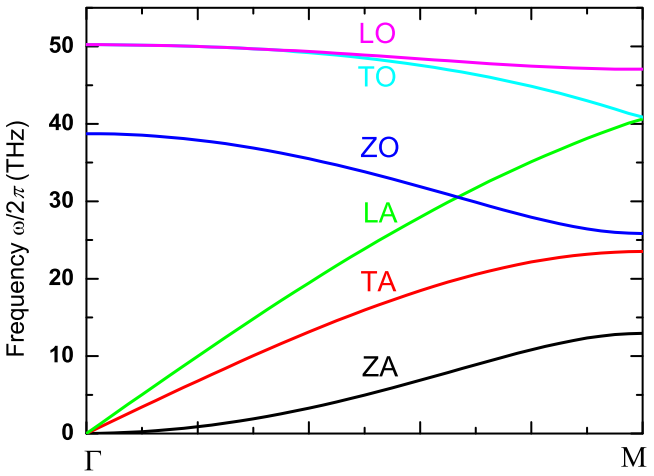

FIG. 4. (Color online) Phonon dispersion relation (Γ-M) in SLG.

modes [15]. Then, we focus on the spectral phonon relaxation times.

The frequency dependent phonon relaxation time τ of the out-of-plane acoustic (ZA), transverse acoustic (TA), and longitudinal acoustic (LA) branches, whose dispersion is shown in Fig. 4, in pristine and 1.1% defected graphene is shown in the upper panel of Fig. 5. The phonon modes are along the direction from Γ to M in the first Brillouin zone (BZ). We note that all the resolvable phonon modes have relaxation time values of below 100 ps. This information supports our finding that the correlation length of 100 ps in the GK method is long enough to get a converged thermal conductivity value. In the pristine graphene, except for low-frequency phonon, τ's of ZA, TA, and LA modes are around 10–30 ps, 5–20 ps, and 3–13 ps, respectively. These values are at the same order but lower than the values from the three-phonon scattering rate calculation based on relaxation time approximation (without iteration) by Lindsay *et al.* [47]. One possible reason is that the reflection symmetry in MD is not fully presented due to the fluctuation of the graphene flake. One other reason may be that the ignorance of the fourth and higher-order phonon-phonon scattering makes the three-phonon scattering rate calculation underestimate the phonon scattering rate.

After introducing 1.1% STW defects, τ's of ZA, TA, and LA modes are reduced by about one order to 0.7–2 ps, 0.5–3 ps, and 0.3–3 ps, respectively. τ of ZA mode suffers the most reduction because the breakdown of reflection symmetry in the out-of-plane direction makes the scattering between ZA mode and in-plane modes unblocked [47]. Generally, the same concentration of DVs gives a similar reduction for ZA mode but a higher reduction for TA and LA modes, compared to STW defects. In the medium-to-high range of frequency, MVs give more reduction than both STW defects and DVs for all the modes.

Distinct from $\tau \sim \omega^{-2}$ in three-dimensional materials [49], τ in the pristine graphene does not show a clear frequency dependence, except for the extremely-low-frequency phonon. After introducing DVs or MVs, τ of all the modes shows a strong dependence on frequency; in contrast, STW defects make little difference on the frequency dependence of τ. This implies that DVs and MVs induce a higher phonon-defect

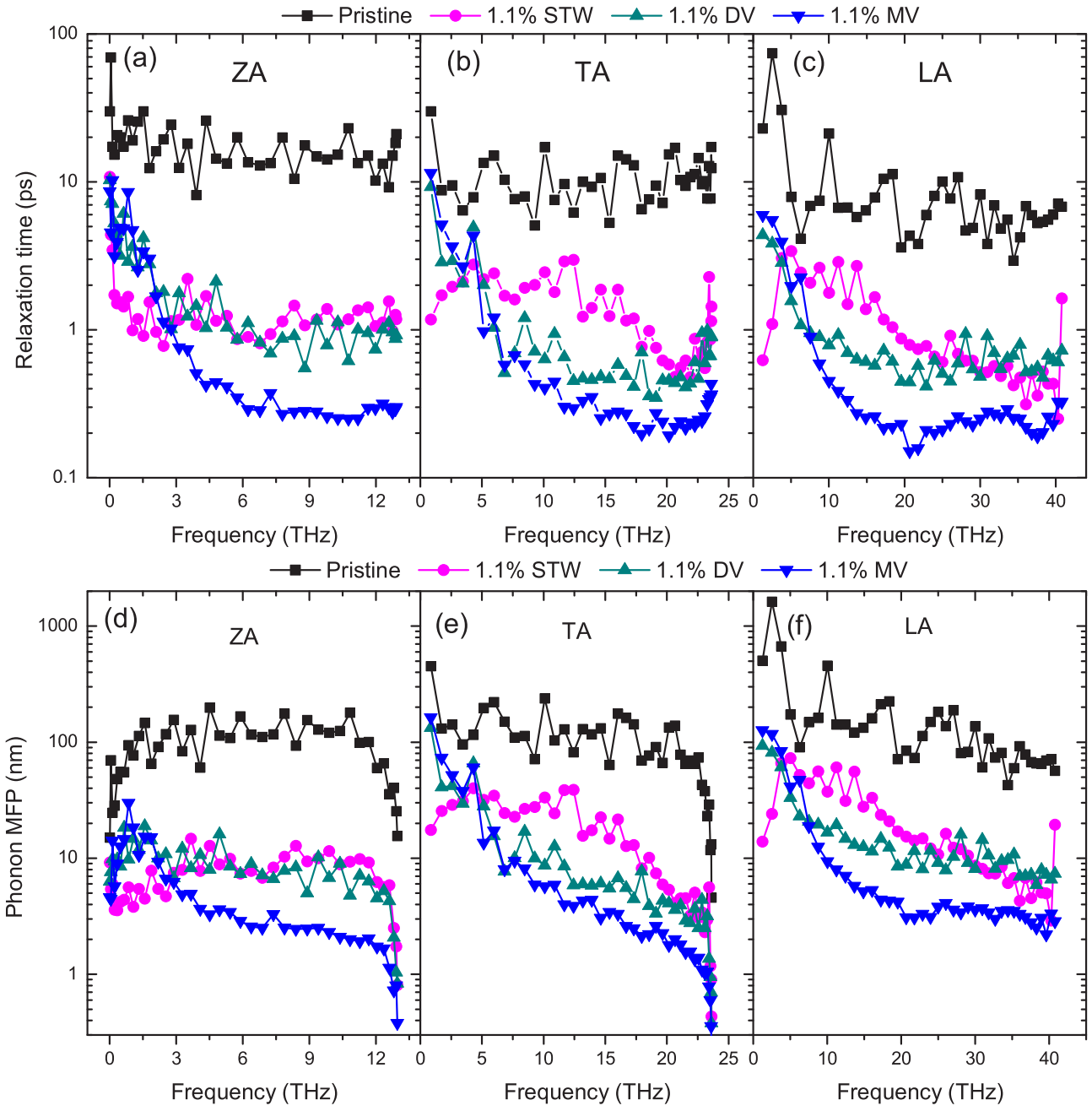

FIG. 5. (Color online) Phonon relaxation time/MFP of (a)/(d) ZA, (b)/(e) TA, (c)/(f) LA modes as a function of frequency (Γ-M) in pristine and 1.1% defected SLG at room temperature.

scattering rate for higher frequency, while the STW defects scatter the phonon more uniformly. Fitting the data gives a phonon-defect scattering rate of $\tau_{p-d}^{-1} \sim \omega^{1.3}$ for DVs and MVs, which gives a critical revisit of the traditionally used $\sim\omega^4$ dependence. Such a difference between the frequency dependencies of the phonon-STW defect and phonon-vacancy defect scattering rates is probably the result of the different local vibration frequencies at the two types of defects. The local phonon frequencies $\omega_{0,\mathrm{STW}}$ at STW defects are close to the intrinsic phonon frequencies ω in graphene since STW defects do not change the number or the mass of the carbon atoms, whereas the local phonon frequencies $\omega_{0,V}$ at vacancies are much higher than the intrinsic phonon frequency ω due to the vibration of atoms neighboring vacancies. Since $\omega_{0,\mathrm{STW}} \approx \omega$, the scattering of the incident phonon by the local phonons at STW defects is described as the Thompson scattering model: The STW defects absorb the incident phonons (ω) from one direction and vibrate at similar frequencies ($\omega_{0,\mathrm{STW}}$), and then they re-emit these vibrations in all directions giving frequency independent scattering. It should be noted, however, that not all the local phonons have similar frequencies with the intrinsic phonons in graphene since some short bonds around the STW defects give a portion of high-frequency phonons as seen in the DOS plot in Fig. 3(b). Due to such high-$\omega_{0,\mathrm{STW}}$ local phonons, the phonon-STW defect scattering is not completely frequency independent as seen in the LA mode in Fig. 5(c). In contrast,

the atoms neighboring vacancies absorb the incident phonons (ω) and vibrate at higher local frequencies $\omega_{0,V} \gg \omega$, giving a strong frequency dependent scattering cross section of $(\frac{\omega}{\omega_{0,V}})^4$ based on the Rayleigh scattering model. It should also be noted that not all the phonons have a wavelength much longer than the defect size. Therefore, the Rayleigh model cannot completely describe the phonon-vacancy scattering, and Mie scattering takes place and reduces the power in the frequency dependence from 4 to 1.1–1.3.

The inaccuracy of $\sim\omega^4$ dependence may arise from two aspects. First, it was derived from the perturbation by mass difference and bond difference introduced by impurity atoms while assuming that the neighbor bonds were not affected. However, in vacancy-defected materials, the modification of the neighbor bonds caused by the missing atoms is not negligible [25]. Second, $\sim\omega^4$ was approximated from $\sim\omega^2 g(\omega)$ by assuming the Debye model with a single phonon branch, i.e., the density of state, was $g(\omega) \sim \omega^2$. However, typically materials have three different acoustic branches with different dispersion relations, and thus the total density of state $g(\omega)$ does not obey the $\sim\omega^2$ dependence even if each branch is linearly dependent on frequency. Besides, as shown in Fig. 4, graphene has a nonlinear dispersion branch (ZA mode) and a low-frequency optical branch (ZO mode) which give significant deviation from $g(\omega) \sim \omega^2$ in the acoustic-frequency range. The phonon-defect scattering rates calculated from NMA for the three types of defects have disclosed the limitation of the traditional formalism and also demonstrated the ability of NMA to calculate phonon-defect scattering rate beyond other current methods. Another interesting find is that the τ's of some low-frequency phonons in MV-defected graphene are close or even higher than those in DV-defected or STW-defected graphene, although the MV-defected graphene owns the lowest thermal conductivity. This is consistent with the conventional assumption that the long-wavelength phonon suffers less scattering by the defects of smaller size in the Rayleigh scattering model.

In the lower panel of Fig. 5, we show the spectral phonon MFP in pristine and 1.1% defected graphene at room temperature. Compared to phonon relaxation time, the information of spectral phonon MFP is of more importance in the point of view of application because phonon MFP directly controls the size effect of samples in experiment. The MFP in pristine graphene predicted from NMA varies from 70 to 1000 nm. We note that the LA mode owns the longest phonon MFP owing to its high group velocity. In contrast, due to the lower group velocity of ZA phonons, the MFP of the ZA mode is not as high as the TA and LA modes although the ZA mode owns a longer relaxation time. The sharp drop of MFP for the low-frequency ZA mode is due to the nonlinear dispersion at the center of the first BZ. The same behavior occurs for high-frequency ZA and TA modes for the same reason at the boundary of the first BZ. After introducing vacancies, the dominant phonon MFP spread over a wider range than that for pristine graphene due to the nonuniform frequency dependent scattering, e.g., less scattering for low-frequency phonon and more scattering for high-frequency phonon. In contrast, STW defects make no significant difference to the breadth of the dominant MFP range because of the nearly uniform defect scattering.

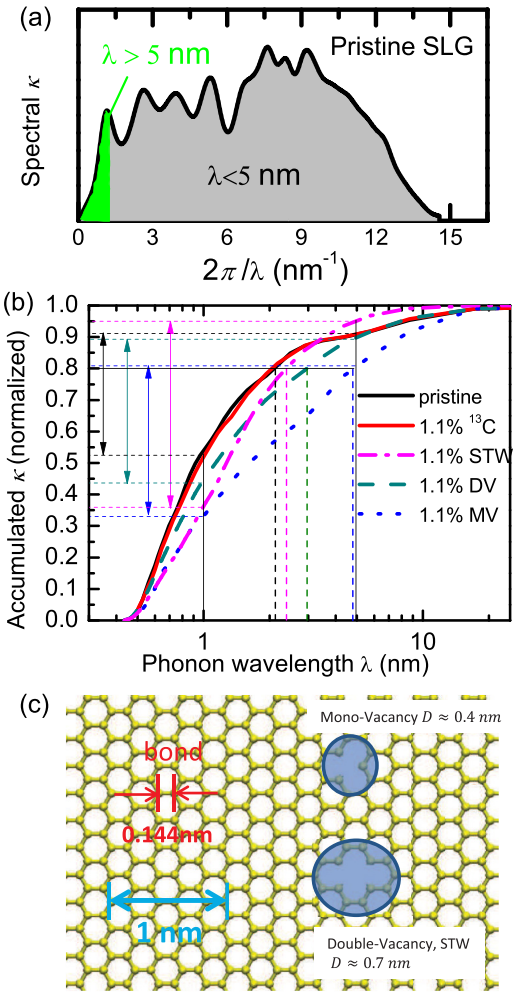

FIG. 6. (Color online) (a) The spectral thermal conductivity of pristine SLG as a function of wave number ($2\pi/\lambda$). (b) The normalized thermal conductivity accumulation with respect to phonon wavelength in pristine and 1.1% defected graphene samples. (c) A sketch illustrating the critical lengths and the sizes of defects in graphene with D representing the approximate diameter.

C. κ accumulation with phonon wavelength

The importance of long-wavelength phonons to thermal transport in pristine SLG has been extensively studied. Nika *et al.* [50] emphasized that the long-wavelength phonons made a significant contribution to the thermal conductivity and its length dependence. Chen *et al.* considered the long-wavelength contribution using Klemens' model [48]. From the point view of kinetic theory [Eq. (4)], the long-wavelength phonon has no significant contribution. As shown in Fig. 6(a), spectral κ as a function of wave number $2\pi/\lambda$, the contribution of long-wavelength phonons, for example $\lambda > 5$ nm, is the green area enclosed by the spectral κ function and the wave-number axis from the origin ($\lambda = \infty$) to 1.26 nm^{-1}. The NMA gives the contribution of this part at about 9% at room temperature. Our result of the small contribution by long-wavelength phonon does not come from the finite size used in MD simulation. If the $\tau \sim \omega^{-2}$ dependence in the long-wavelength limit (LWL) is valid, then Eq. (4) gives an infinite thermal conductivity value since $\int_0^{k_{\max}} \frac{1}{k} dk$

TABLE I. The relative contribution to κ in pristine and 1.1% defected SLG samples from the phonons with short, medium, and long wavelength.

Samples	Short λ (0,1 nm)	Medium λ (1 nm,5 nm)	Long λ (5 nm, $+\infty$)
Perfect SLG	52%	39%	9%
1.1% STW	35%	60%	5%
1.1% DV	44%	45%	11%
1.1% MV	33%	47%	20%
0.5% MV	33%	49%	18%
0.2% MV	38%	48%	14%

does not converge. Thus, the relation $\tau \sim \omega^{-2}$ is invalid in the LWL, and the lifetime is finite in the LWL, which has been shown numerically by Bonini *et al.* [51] by directly calculating the scattering rate in suspended graphene using anharmonic lattice dynamics. This conclusion is essentially important since it implies that the thermal conductivity integral [Eq. (4)] starts from the origin (zero times a finite number gives zero). Thus, our simulation size (about 17 nm, e.g., the longest wavelength that can be captured) is sufficient for the spectral κ being extrapolated to the origin, as shown in Fig. 6(a), and to demonstrate the small contribution by long-wavelength phonons. This contribution is probably not significant even if the spectral κ is calculated from any other method, since mathematically the area representing this contribution only covers a very small range of wave number as shown in Fig. 6(a), and the curve of the spectral κ has to start from the origin. Physically this is because the density of states in the long-wavelength range is extremely low.

After introducing defects, the relative contributions of the phonons in various wavelength ranges vary with the defect types. According to the normalized thermal accumulation as a function of phonon wavelength in Fig. 6(b), the relative contributions of short-wavelength ($\lambda < 1$ nm), medium-wavelength ($1\text{ nm} < \lambda < 5\text{ nm}$), and long-wavelength ($\lambda > 5$ nm) phonons are listed in Table I. Generally the relative contribution of short-wavelength phonons decreases after introducing defects, indicating the short-wavelength phonons are scattered more than medium-to-long-wavelength phonons by the defects. This is because the sizes of the defects are below 1 nm, as shown in Fig. 6(c). Nevertheless, the contribution of short-wavelength phonons is still more than 30%. Relatively, the contribution of medium-wavelength phonon increases, especially in STW-defected graphene. We note that, even in MV-defected graphene, the short-wavelength phonon is severely scattered, and the contribution of long-wavelength phonon is still not significant (~20%). This is consistent with our previous analysis. Another interesting finding is that although STW defect is not as efficient as vacancy in reducing thermal conductivity, it is more effective in suppressing long-wavelength phonons (also seen in Fig. 5).

D. κ accumulation with phonon mean free path

In Fig. 7(a), we compare the normalized thermal conductivity accumulation with respect to the phonon MFP in pristine and 1.1% defected graphene. The phonon with a

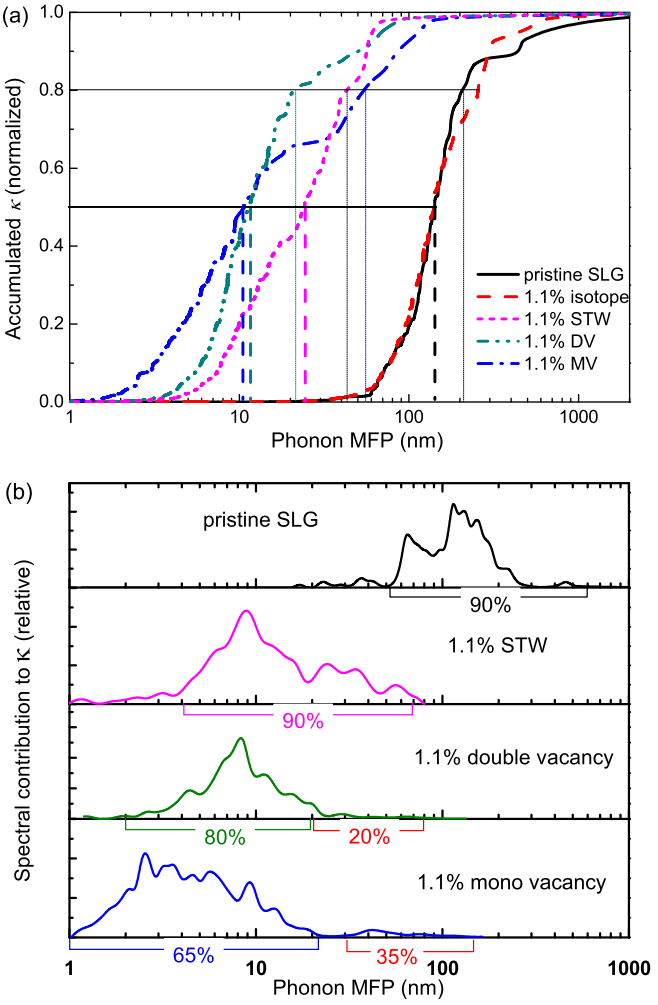

FIG. 7. (Color online) (a) Normalized spectral phonon conductivity and (b) its accumulation with respect to phonon MFP in pristine and 1.1% defected graphene samples at room temperature.

MFP of 70–500 nm is found to contribute 90% of the total κ in pristine graphene. To compare with experiment, the effective MFP calculated from the measured κ values varies in a vast range of 240–600 nm (500–1000 nm for backscattering MFP) [10,43,46]. 1.1% STW defects, DVs, and MVs are found to reduce the dominant MFP to 4–70 nm, 2–80nm, and 1–130 nm, respectively. The information of the effective MFP is far from enough to grasp the entire understanding of the phonon transport. For instance, we note that the MV-defected graphene has more long-MFP phonon than the other two defected graphene samples although MV-defected graphene has the lowest effective MFP and κ. The contribution of long-MFP phonon in MV-defected graphene is seen more clearly in the spectral thermal conductivity plots [see Fig. 7 (b)]. The long-MFP phonon (20–80 nm) in DV-defected graphene contributes 20%, while the counterpart in MV-defected graphene has longer MFP at about 25–150 nm and more contribution to κ at about 35%. The long phonon MFP in MV-defected graphene is due to the smaller size of the defect and thus less scattering for the long-wavelength phonon.

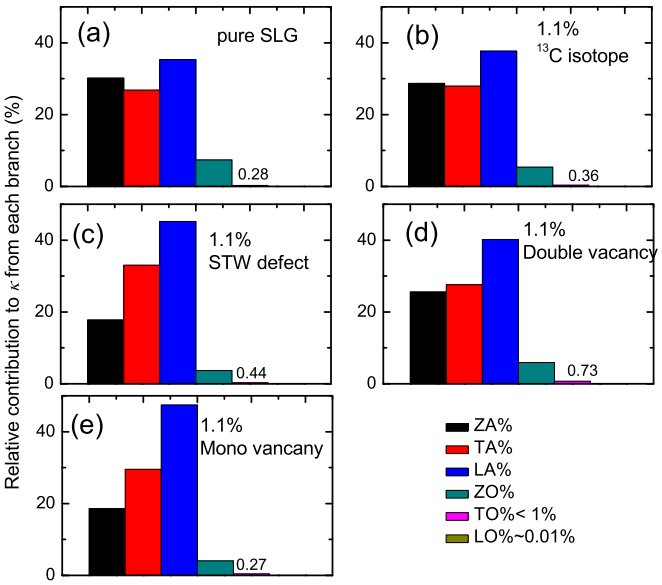

FIG. 8. (Color online) The relative contribution of each phonon branches to the total thermal conductivity in (a) pristine SLG, (b) 1.1% isotope-doped SLG, (c) 1.1% STW-defected SLG, (d) 1.1% DV-defected SLG, and (e) 1.1% MV-defected SLG at room temperature.

E. Relative importance of phonon branches

The understanding of relative importance of different phonon branches in thermal transport is important in thermal engineering. The relative contribution of each branch to total thermal conductivity of pristine SLG has been studied in many papers and summarized in Refs. [23,41,52]. Within the framework of anharmonic lattice dynamics (ALD) and three-phonon scattering, Lindsay *et al.* [47] found that the reflection symmetry in the out-of-plane (z) direction forbids about 60% scattering between the out-of-plane modes and the in-plane modes, and thus makes the ZA mode dominate the thermal transport. In contrast, the normal mode analysis combined shows that the relative contribution of ZA mode is around 30% as shown in Fig. 8(a), akin to Qiu and Ruan's results [40]. Lindsay *et al.* attribute this discrepancy to the presence of normal (N) scattering which is excluded in the iterative three-phonon calculation. This discrepancy may also come from the essential difference between three-phonon calculation and MD simulation. In ALD calculation, the graphene sheet remains a perfect plane with the reflection symmetry perfectly preserved, while in MD simulations the atoms are not at their equilibrium positions and the graphene is not a plane, as a result the reflection symmetry may not be well presented in MD simulations. Another possible cause that may bring the contribution of ZA mode down in ALD calculation is including the fourth and higher orders of phonon scatterings. The relative contributions of other modes from NMA [Fig. 8(a)] are TA $\approx$ 27%, LA $\approx$ 35%, and ZO $\approx$ 7%, respectively, differing considerably from the results of 15%, 9%, and 0 from ALD calculation by Lindsay *et al.* [47].

By introducing defects, the relative importance of different phonon branches changes remarkably. Figures 8(b)–8(e) show the relative contributions in isotope-doped, STW-defected, double-vacancy defected, and monovacancy defected graphene, respectively, with the concentration of 1.1%. ZA, TA, and LA modes dominate the thermal transport in all samples, and the contribution from TO and LO modes are negligible (<1%). The contribution of all phonon modes are reduced after introducing isotopes or defects because of the phonon-isotope or phonon-defect scattering. Generally, ZA and ZO modes are reduced the most due to the breakdown of reflection symmetry in the z direction so that the relative contributions of ZA and ZO modes decrease while those of TA and LA modes increase. Isotopes have the least modification to the relative contribution of each branch, while STW defects and MVs have the most. Specifically, in STW-defected and MV-defected graphene, the relative contribution of the ZA mode is reduced to less than 20% while that of the LA mode is increased to almost 50%. It is interesting that DVs only give a slight modification to the relative contribution of each branch although κ is significantly reduced, indicating that DVs induce similar phonon scattering rates for the in-plane and the out-of-plane modes.

IV. EFFECT OF DEFECT CONCENTRATION

Taking MV graphene as an example, the impact of defect concentration on the spectral phonon transport properties is studied. In Fig. 9, we compare the spectral phonon relaxation time and MFP (Γ-M) for ZA, TA, and LA modes in pristine, 0.2%, 0.5%, and 1.1% MV-defected graphene. We find that the phonon-defect scattering rate $\tau_{p-d}^{-1} \sim \omega^{1.1-1.3}$ works well for all these concentrations and phonon branches. The medium-to-high-frequency phonons are found to have 10-fold, 20-fold, and 40-fold reduction in relaxation times and MFP for 0.2%, 0.5%, and 1.1% MV-defect graphene samples, respectively. The reduction for low-frequency phonons is not that much and has only a slight increase with increasing vacancy concentration. The phonons whose wavelength is much shorter than the average distance between two vacancies "view" the vacancies as independent scattering centers, and thus the total scattering cross sections, or scattering rates, for those phonons increase linearly with increasing vacancy concentration. In contrast, phonons of much longer wavelength "see" the material more as a homogeneous medium rather than individual scattering centers. Therefore, the total scattering rates of those long-wavelength phonons increase more slowly with increasing vacancy concentration. In general, this is also why the reduction of thermal conductivity of materials by increasing doping becomes less efficient as the doping concentration increases. As a result, long-wavelength phonons play a more important role in thermal transport as vacancy concentration increases according to the κ accumulation with the phonon wavelength, as shown in Fig. 10(a). 80% of κ is contributed from phonons with λ shorter than 2 nm, 3.7 nm, 4.5 nm, and 4.8 nm in the pristine, 0.2%, 0.5%, and 1.1% MV defected graphene samples, respectively. Phonons with $\lambda > 5$ nm contribute 9%, 14%, 18%, and 20% of κ in these samples, respectively, as listed in Table I. The accumulated κ and the relative thermal conductivity κ/κ_0 [the inset in Fig. 10(a)] vary more slowly as vacancy concentration increases.

Similarly, the κ accumulation with the phonon MFP in these graphene samples are calculated, as shown in Fig. 10(b). The curves move towards the short MFP side as the vacancy

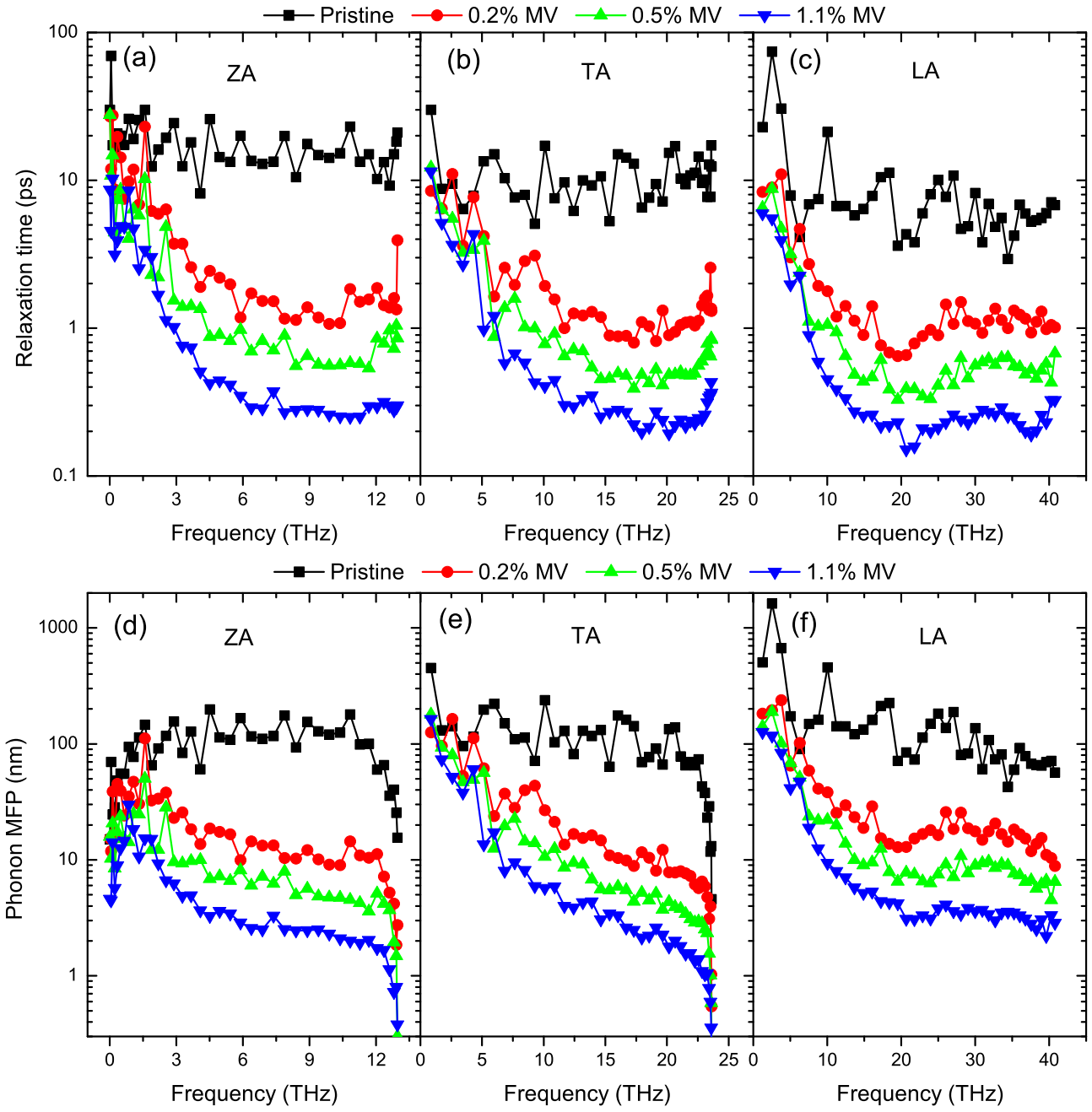

FIG. 9. (Color online) The phonon relaxation time/MFP of (a/d) ZA, (b/e) TA, and (c/f) LA modes as a function of frequency (Γ-M) in pristine and MV-defected SLG at room temperature.

concentration increases. Nevertheless, the phonons with MFP of 40–200 nm keep contributing 30% to total κ even when the vacancy concentration increases. Figure 10(c) demonstrates the comparison between pristine, 0.2% MV-graphene, 0.5% MV-graphene, and 1.1% MV-graphene samples in the relative contribution distributions in different phonon branches. As the vacancy concentration increases, the relative importance of ZA and ZO modes decreases while that of the LA mode increases. The relative contribution of the TA mode almost keeps a constant at around 30%. With increasing vacancy concentration, the distribution of relative contribution in different phonon branches varies more slowly and trends to a limit at ZA $\sim$ 16%, TA $\sim$ 30%, and LA $\sim$ 54%.

V. SUMMARY

In this paper, we have demonstrated NMA on the study of phonon-defect scattering and compare the impact of STW defect, DV, and MV on the spectral phonon transport in graphene. We find that the phonon-STW defect scattering rate has no significant frequency dependence, and as a result the relative contribution of long-wavelength phonons sharply decreases. In contrast, the phonon-defect scattering rate by DVs or MVs follows $\tau_{p-d}^{-1} \sim \omega^{1.1-1.3}$ dependence, which deviates from the conventionally used Rayleigh scattering rate of $\sim\omega^4$. The inaccuracy of the latter arises from 1) the ignorance of neighbor-bond modification around the defects

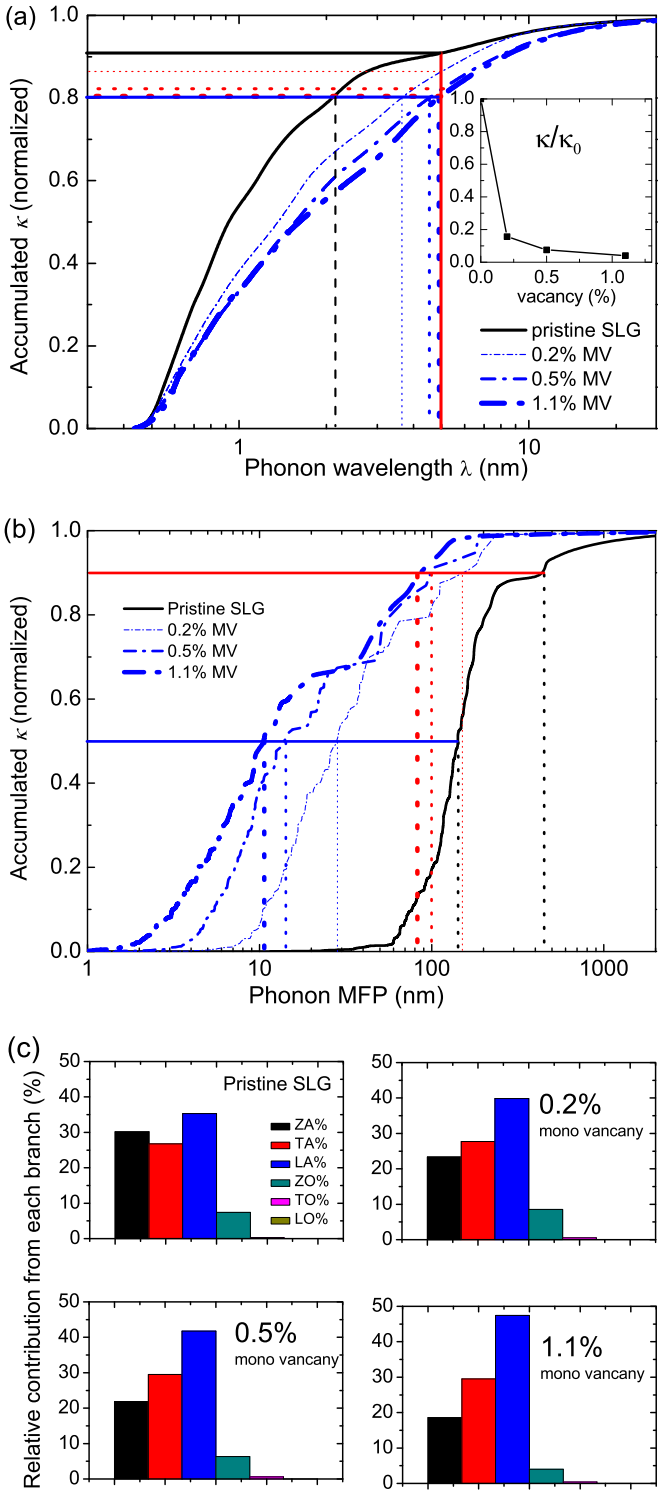

FIG. 10. (Color online) The normalized thermal conductivity accumulation with respect to (a) phonon wavelength and (b) phonon MFP in the graphene samples with 0, 0.2%, 0.5%, and 1.1% MVs at room temperature. (c) Relative contribution to thermal conductivity from each branch. The inset in (a) shows κ/κ_0 as a function of vacancy concentration.

and 2) the inaccuracy of the single-acoustic-mode Debye model. The NMA predicts a contribution of 9% from the phonons with a wavelength longer than 5 nm for pristine graphene. As vacancies are introduced, the contribution from this range of phonons increases, but it is still no more than 20%. From the kinetic theory we demonstrate that the low contribution of long-wavelength phonon is due to the low density of states. Another interesting finding is that although MV-defected graphene has the lowest thermal conductivity as compared to the other two defected graphene samples at the same defect concentration, it has a portion of phonons with the longest MFP. This is consistent with the Rayleigh scattering picture in that the scattering cross section for a long wavelength decreases with decreasing scatterer size. We also note that the contribution from the long MFP and long wavelength phonon does not decrease much as the vacancy concentration increases. As for different phonon branches, the relative contribution from the out-of-plane branches decreases as STW defects or MVs are introduced. As the concentration of MV increases, the relative contribution from the out-of-plane modes keeps decreasing while that of the TA mode almost keeps a constant at around 30%. In contrast, the relative contribution from each branch changes little after introducing DV defects.

The STW, DV, and MV defects can modify the local electronic band structure near Dirac points. For example, based on the previous studies [53–55], STW defects may shift the degenerate point slightly from the K point and may also open a small band gap, whereas DVs and MVs can open a band gap of 0.015 eV and 0.1 eV, respectively. The combination of those defects may generate a large band gap of 0.3 eV. These results illustrate that point defects may endow graphene with semiconductor behavior like graphene nanostructures, e.g., GNR, graphene nanomesh, nanoporous graphene, etc. Such semiconductor behavior combined with the reduced thermal conductivity may benefit the thermoelectric properties of graphene.

The capability of NMA is not limited to the three types of defects discussed in this paper. For other defects such as multibond distortion, substitutional atoms, small pores, and adhered metal or hydrogen atoms [1], the NMA method probably works well as long as the perturbation caused by the defects is not large. Besides, it is very convenient to study phonon MFP and thermal conductivity in other more complicated structures using our results of phonon scattering rate $\tau^{-1}_{d-\mathrm{SLG},\mathbf{k},\nu}$ in defected SLG. For instance, in defected graphene nanoribbon (d-GNR), a potential thermoelectric material [14,56], the spectral phonon scattering rate $\tau^{-1}_{d-\mathrm{GNR},\mathbf{k},\nu}$ may be calculated by simply adding a boundary scattering term to $\tau^{-1}_{d-\mathrm{SLG},\mathbf{k},\nu}$ as

$$\tau^{-1}_{d-\mathrm{GNR},\mathbf{k},\nu} = \tau^{-1}_{d-\mathrm{SLG},\mathbf{k},\nu} + \frac{2|v_{\mathbf{k},\nu,\perp}|}{W}\frac{1-p}{1+p}. \qquad (7)$$

Here $0 \leqslant p \leqslant 1$ is the specularity parameter [57], W is the width of the GNR, and $v_\perp$ is the group velocity perpendicular to the edges. Typically the value of p is about 0.95 in GNR with smooth edges [22]. The limitation [23] of NMA lies in the classical feature of MD where quantum correction is required [58]. As for the method of frequency domain NMA, another form without using eigenvectors is also valid and can be used [59].

ACKNOWLEDGMENTS

The work was partially supported by the National Science Foundation (Grant No. 1150948). We would like to thank Bo Qiu and Prabhakar Marepalli for sharing some codes. Suggestions from Yan Wang and Frank Brown are gratefully appreciated. Simulations were performed at the Purdue Network for Computational Nanotechnology (NCN). Z.Y. and B.C. acknowledge partial support from the National Natural Science Foundation of China (No. 51322603) and the Program for New Century Excellent Talents at the University of China.

[1] F. Banhart, J. Kotakoski, and A. V. Krasheninnikov, ACS Nano **5**, 26 (2011).
[2] A. Stone and D. Wales, Chem. Phys. Lett. **128**, 501 (1986).
[3] A. Hashimoto, K. Suenaga, A. Gloter, K. Urita, and S. Iijima, Nature (London) **430**, 870 (2004).
[4] M. H. Gass, U. Bangert, A. L. Bleloch, P. Wang, R. R. Nair, and A. K. Geim, Nat. Nanotechnol. **3**, 676 (2008).
[5] J. C. Meyer, C. Kisielowski, R. Erni, M. D. Rossell, M. F. Crommie, and A. Zettl, Nano Lett. **8**, 3582 (2008).
[6] J. H. Warner, M. H. Rümmeli, L. Ge, T. Gemming, B. Montanari, N. M. Harrison, B. Büchner, and G. A. D. Briggs, Nat. Nanotechnol. **4**, 500 (2009).
[7] C. Girit, J. Meyer, R. Erni, and M. Rossell, Science **323**, 1705 (2009).
[8] M. M. Ugeda, I. Brihuega, F. Guinea, and J. M. Gómez-Rodríguez, Phys. Rev. Lett. **104**, 096804 (2010).
[9] L. Tapasztó, G. Dobrik, P. Nemes-Incze, G. Vertesy, P. Lambin, and L. P. Biró, Phys. Rev. B **78**, 233407 (2008).
[10] Y. Xu, Z. Li, and W. Duan, Small **10**, 2182 (2014).
[11] G. Chen and A. Shakouri, J. Heat Transfer **124**, 242 (2002).
[12] M. T. Lusk and L. D. Carr, Phys. Rev. Lett. **100**, 175503 (2008).
[13] G. Xie, R. Yang, P. Chen, J. Zhang, X. Tian, S. Wu, J. Zhao, M. Cheng, W. Yang, D. Wang, C. He, X. Bai, D. Shi, and G. Zhang, Small (Weinheim an der Bergstrasse, Germany) **10**, 2280 (2014).
[14] P.-H. Chang, M. S. Bahramy, N. Nagaosa, and B. K. Nikolić, Nano Lett. **14**, 3779 (2014).
[15] H. Zhang, G. Lee, and K. Cho, Phys. Rev. B **84**, 115460 (2011).
[16] F. Hao, D. Fang, and Z. Xu, Appl. Phys. Lett. **99**, 041901 (2011).
[17] B. Mortazavi and S. Ahzi, Carbon **63**, 460 (2013).
[18] J. Haskins, A. Kınacı, C. Sevik, H. Sevinçli, G. Cuniberti, and T. Çağın, ACS Nano **5**, 3779 (2011).
[19] J. J. Yeo, Z. Liu, and T. Y. Ng, Nanotechnology **23**, 385702 (2012).
[20] J.-W. Jiang, B.-S. Wang, and J.-S. Wang, Appl. Phys. Lett. **98**, 113114 (2011).
[21] P. Scuracchio, S. Costamagna, F. M. Peeters, and A. Dobry, Phys. Rev. B **90**, 035429 (2014).
[22] Y. Wang, B. Qiu, and X. Ruan, Appl. Phys. Lett. **101**, 013101 (2012).
[23] T. Feng and X. Ruan, J. Nanomaterials **2014**, 206370 (2014).
[24] P. G. Klemens, *Solid State Physics*, edited by F. Seitz and D. Turnbull (Academic Press, New York, 1958), Vol. 7, p. 1.
[25] P. Klemens, Proc. Phys. Soc., London, Sect. A **68**, 1113 (1955).
[26] P. Klemens and D. Pedraza, Carbon **32**, 735 (1994).
[27] C. A. Ratsifaritana and P. G. Klemens, Int. J. Thermophys. **8**, 737 (1987).
[28] G. Xie, Y. Shen, X. Wei, L. Yang, H. Xiao, J. Zhong, and G. Zhang, Sci. Rep. **4**, 5085 (2014).
[29] J. A. Thomas, J. E. Turney, R. M. Iutzi, C. H. Amon, and A. J. H. McGaughey, Phys. Rev. B **81**, 081411 (2010).
[30] A. J. C. Ladd, B. Moran, and W. G. Hoover, Phys. Rev. B **34**, 5058 (1986).
[31] N. de Koker, Phys. Rev. Lett. **103**, 125902 (2009).
[32] A. J. H. McGaughey and M. Kaviany, Phys. Rev. B **69**, 094303 (2004).
[33] M. T. Dove, *Introduction to Lattice Dynamics* (Cambridge University Press, New York, 1993).
[34] S. Plimpton, J. Comp. Phys. **117**, 1 (1995).
[35] L. Lindsay and D. A. Broido, Phys. Rev. B **81**, 205441 (2010).
[36] J. Tersoff, Phys. Rev. B **39**, 5566 (1989).
[37] A. J. H. McGaughey and M. Kaviany, Adv. Heat Transfer **39**, 169 (2006).
[38] V. K. Tewary and B. Yang, Phys. Rev. B **79**, 125416 (2009).
[39] A. Maiti, G. Mahan, and S. Pantelides, Solid State Commun. **102**, 517 (1997).
[40] B. Qiu and X. Ruan, arXiv:1111.4613v1.
[41] Y. Wang, A. K. Vallabhaneni, B. Qiu, and X. Ruan, Nanoscale Microscale Thermophys. Eng. **18**, 155 (2014).
[42] S. Ghosh, W. Bao, D. L. Nika, S. Subrina, E. P. Pokatilov, C. N. Lau, and A. A. Balandin, Nat. Mater. **9**, 555 (2010).
[43] S. Ghosh, I. Calizo, D. Teweldebrhan, E. P. Pokatilov, D. L. Nika, A. A. Balandin, W. Bao, F. Miao, and C. N. Lau, Appl. Phys. Lett. **92**, 151911 (2008).
[44] S. Chen, A. L. Moore, W. Cai, J. W. Suk, J. An, C. Mishra, C. Amos, C. W. Magnuson, J. Kang, L. Shi, and R. S. Ruoff, ACS Nano **5**, 321 (2011).
[45] C. Faugeras, B. Faugeras, M. Orlita, M. Potemski, R. R. Nair, and A. K. Geim, ACS Nano **4**, 1889 (2010).
[46] X. Xu, L. F. C. Pereira, Y. Wang, J. Wu, K. Zhang, X. Zhao, S. Bae, C. Tinh Bui, R. Xie, J. T. L. Thong, B. H. Hong, K. P. Loh, D. Donadio, B. Li, and B. Özyilmaz, Nat. Commun. **5**, 3689 (2014).
[47] L. Lindsay, D. A. Broido, and N. Mingo, Phys. Rev. B **82**, 115427 (2010).
[48] S. Chen, Q. Wu, C. Mishra, J. Kang, H. Zhang, K. Cho, W. Cai, A. A. Balandin, and R. S. Ruoff, Nat. Mater. **11**, 203 (2012).
[49] M. Holland, Phys. Rev. **132**, 2461 (1963).
[50] D. L. Nika, S. Ghosh, E. P. Pokatilov, and A. A. Balandin, Appl. Phys. Lett. **94**, 203103 (2009).
[51] N. Bonini, J. Garg, and N. Marzari, Nano Lett. **12**, 2673 (2012).
[52] D. L. Nika and A. A. Balandin, J. Phys.: Condens. Matter **24**, 233203 (2012).
[53] J. Kang, J. Bang, B. Ryu, and K. J. Chang, Phys. Rev. B **77**, 115453 (2008).

[54] J. M. Carlsson and M. Scheffler, Phys. Rev. Lett. **96**, 046806 (2006).
[55] D. J. Appelhans, L. D. Carr, and M. T. Lusk, New J. Phys. **12**, 125006 (2010).
[56] H. Sevinçli, C. Sevik, T. Çağın, and G. Cuniberti, Sci. Rep. **3**, 1228 (2013).
[57] Z. Aksamija and I. Knezevic, Phys. Rev. B **82**, 045319 (2010).
[58] J. E. Turney, A. J. H. McGaughey, and C. H. Amon, Phys. Rev. B **79**, 224305 (2009).
[59] T. Feng, B. Qiu, and X. Ruan, J. Appl. Phys. **117**, 195102 (2015).